A Probabilistic Method to Construct an Optimal Ice Chronology for Ice Cores

Benedicte Lemieux-Dudon, [1] Parrenin Frederic, [1] Eric Blayo [2]

[1] *LGGE CNRS, BP 96, F-38402 Saint-Martin d'Hères Cedex, France, lemieux@lgge.obs.ujf-grenoble.fr*

[2] *LJK, BP 53, F-38041 Grenoble Cedex, France*

Abstract: Accurate ice chronologies are needed for the interpretation of paleoclimate reconstructions inferred from ice cores. Several methods are used to provide chronological information: identification of dated horizons along the cores, synchronization to other dated paleoclimatic records, counting of annual layers or modelling of the ice flow. These methods are relevant for different parts of the core and enable to reach various levels of accuracy. We present a probabilistic approach based on inverse techniques which aims at building an optimal ice core chronology by using all the available chronological information. It consists in identifying the accumulation rate and the thinning function along the core 1) which are as close as possible to the flow model simulations and 2) so that the corresponding ice chronology is as close as possible to independent dating information. This probabilistic approach enables to evaluate confidence intervals on the optimal age scale as well as on the accumulation and the thinning estimates. We test the new method on the EPICA Dome C ice core. The necessary prior accumulation rate and thinning function as well as a set of dated horizons are provided by a previous work aiming at the EDC3 age scale reconstruction. We further discuss the sensitivity of the obtained optimal solution with respect to the necessary prior information. This probabilistic approach could be used in the future to build a common and optimal chronology for several ice cores simultaneously.

Key words: Inverse Methods, Ice Core Chronology, Paleo-climate.

1 Introduction

Deep ice cores extracted from Antarctica or Greenland recorded a wide range of past climatic events [8, 9]. Physico-chemical measurements on the core material provide many types of record. For instance the past temperature changes are inferred from ice isotopes and the past atmospheric composition is deduced from the analysis of trapped air bubbles. These records are valuable archives to understand past climatic mechanisms at hand on Earth. To achieve such a goal, accurate ice core chronologies (e.g. a depth-age relationship) are necessary.

For that purpose, one may distinguish the accuracy on "absolute ages" attached to specific events from the accuracy on "event durations". Both types of accuracy are required and they are of course strongly linked but one must keep in mind that an accurate age scale in event duration may misjudge the timing of some events and vice versa. For instance, dating methods providing a precise estimate of event duration may induce an age scale with cumulative errors with depth. On the other hand, some other methods providing an age scale with a good accuracy on absolute ages may imply some distortions on short time intervals.

The currently used methods aiming at ice core dating may fall into four groups: (1) the wiggle matching on other dated time series, (2) the use of dated horizons, (3) the counting of annual layers and (4) the ice flow modelling. We hereafter bring details on each group on the basis of examples.

In the first group one can mention the orbital tuning which consists in the comparison of ice core records to insolation variations [7]. It can apply to the whole core as long as the stratigraphy is preserved [1]. The accuracy in terms of event duration as well as in terms of absolute age is limited because the orbital tuning procedure relies on the assumption of a constant phase between climate (recorded in ice cores) and insolation. One advantage is however that the achieved accuracy does not diminish with depth (assuming steady underlying mechanisms) and it is therefore the currently most precise method to date the bottom of deep ice cores. In this first group, one can also mention the comparison of ice core records to paleoclimatic archives dated with radiochronologic techniques as for instance the U-Th dated speleothems [21]. On the contrary, this later technique is rather relevant for recent periods where radiometric methods apply.

In the second group, one can mention volcanic horizons which provide very accurate age markers in terms of absolute age. This is the case for the last millennium [20], but beyond that limit, accurate absolute ages are associated to very few eruptions [12].

The third group refers to layer-counted chronologies which rely on the recognition of seasonal variations in various records. The new GICC05 chronology for Greenland [18] uses an improved multi-parameters counting

approach, and currently extends back to around 42 kyr BP with a maximum counting error of 4 to 7% during the last glacial period. If this technique is very accurate for estimating the event durations the error on absolute ages however increases with depth.

The last group consists in dating the cores with ice flow modelling. This later method is based on the estimate of $S(z)$, the snow accumulation rate at the deposition time on the ice-sheet surface (expressed in cm of pure ice per year) as well as on the estimate of $T(z)$, the so-called thinning function which is the ratio of a layer thickness at depth z to its initial thickness at the surface. It enables to determine $\chi(z)$ the age of the ice, by depth-integrating the number of annual layers per meter from the surface to the depth z:

$$\chi(z) = \int_0^z \frac{D(z')}{S(z')\,T(z')} dz' \qquad (1)$$

where $D(z)$ is the relative density with respect to pure ice. The parameter $D(z)$ is usually well-known because it is measured with high precision along the drilled ice core [1]. The accumulation rate $S(z)$ is generally inferred from a sedimentation model which uses temperature reconstructions obtained from isotopic analysis of the ice [14]. Finally, the thinning function $T(z)$ is usually estimated by local flow description [14]. However, some poorly known parameters of the flow models within which is incorporated the accumulation model (e.g. basal conditions like the sliding or the melting at the ice/bedrock interface) makes the modelling exercise less accurate with increasing depth and the simplified description most often fails to reproduce the flow behavior all along the core (especially near the bedrock).

To put together all these different chronological information, Parrenin et al. [15] developed an inverse approach which has been used to construct age scales for the East Antarctic and the Greenland ice cores [4, 16, 14, 17]. This inverse approach is solved by a Monte Carlo sampling method (see Mosegaard and Tarantola [11] or Tarantola [19]) which optimally identifies the poorly known parameters of the flow models by the use of data constraint (e.g. dated horizons).

The previous method however suffers from a strong restriction precisely because the involved flow models, apart from their poorly-known parameters are supposed to be perfect. In other words, the modelling uncertainties due to undescribed or unknown physical mechanisms are not considered (e.g. changes of ice mechanical properties, uncertainty in lateral boundary conditions,...etc.). One consequence is that even after appropriate tuning, the model is sometimes unable to capture complex flow behavior and to reproduce the observations, especially for basal ice where the flow becomes more irregular and the model approximations less applicable [1, 13]. Another impact of the above mentioned restriction concerns the confidence intervals on the optimized age scale. They cannot be properly estimated because the sources of uncertainties which are linked to the model imperfections are neglected.

The EDC3 age scale may be taken as an illustration. It was partially built with the above described inverse approach [13] but because of the depicted restriction, the Monte Carlo optimized age scale could not fit all the available age markers. A subset of them was therefore subjectively chosen for constraining the flow parameters [13] and an a posteriori correction was finally applied on a portion of the optimized age scale to circumvent the problem [1, 13]. At last, the EDC3 age scale confidence intervals were only roughly estimated on the basis of the quality of the surrounding age markers.

The current methodological article describes a rigorous method which enables to derive an optimal ice chronology without any a posteriori corrections and where the poorly-known physical mechanisms are statistically considered by the mean of correction functions. The aim is to identify the best corrections on the accumulation rate and on the thinning function which are on one hand consistent with the flow model simulations and on the other hand which induce an age scale and flow entities in best agreement with independent observations. This method moreover enables to rigorously estimate the confidence intervals on the optimized chronology.

In section 2, we describe this new method. Section 3 is devoted to validate the method with experiments on the EPICA DOME C core (hereafter EDC). We construct an optimal age scale by integrating the same elements used for building the EDC3 age scale (i.e. flow model simulation and age markers) and we estimate the associated confidence intervals. We then test the sensitivity of the method with respect to the prior information which is necessary to run the method and finally we discuss the results after the application section.

2 Method

The accumulation rate S and the thinning function T, are key entities of flow models because they enable to calculate the ice chronology with equation (1). Several modelling works targeting a particular drilling site already allowed to estimate these flow entities [14, 5]. Taking the EDC3 age scale as illustration, we underlined in the introduction that these estimates may fail to reproduce some flow irregularities and are at the root of inaccurate ice age reconstructions, mainly because some physical mechanisms are not described in the flow models. This study does not propose itself to enrich the flow description in order to improve these estimations but it is rather a pragmatic approach that aims by the use of data constraints, at identifying the best perturbations on already estimated accumulation rates and thinning functions. The searched perturbations are hereafter called *correction functions* and designated by X. They have the vocation to encompass all sources of modelling uncertainties. In other words, they can either account for errors

[1] $D(z)$ is quickly increasing from around 0.35 for light snow at surface to around 1 at 200 m.

on physical parameters that are already included in the flow modelling or also account for errors due to omitted physical mechanisms.

Inverse techniques provide the rigorous framework to identify X. In the current study, we opt for a *Bayesian* approach [19, 11, 6]. We further decide to use the *Maximum Likelihood* [19] as *optimality criterion* which we investigate by the mean of a variational technique [6] rather than by the use of a Monte Carlo method [10, 19, 11] [2]. The *Bayes theorem* [19, 11, 6] enables to operate a conjunction of the statistical information brought by: 1) the prior knowledge on X which is provided by the flow modelling and (2) some independent observations [3] named Y and their adequacy with the predictions operated by the *observation model* $h(X)$. The *cost function* $J(X)$ is finally derived from the model and data probability conjunction on which is applied the optimality criterion. At last, the J cost function is optimized and provides $X = \hat{X}$ the "optimal" perturbations on T and S.

In the next sections, we first define precisely what are the searched correction functions and second we give all the elements to build the J cost function.

2.1 Correction functions

Let us designate by S^b and T^b, the necessary first guesses on the accumulation rate and on the thinning function which are provided by direct or already optimized flow model simulations. X may be split into two correction functions α and β which target S^b for the former and T^b for the latter:

$$X = (\alpha, \beta)^T \tag{2}$$

The $\alpha(z)$ and $\beta(z)$ correction functions are chosen as multiplicative factors:

$$\alpha(z) = \frac{S^b(z)}{S(z)} \tag{3}$$

$$\beta(z) = \frac{T^b(z)}{T(z)} \tag{4}$$

It must be emphasized that both must be strictly positive. This positive constraint is prescribed by the Eulerian formulation of the age model (1) where neither the thinning function nor the sedimentation rate can be negative or zero, at the risk of producing a discontinuity. Such non-negative physical entities are called Jeffrey's variables (see Mosegaard and Tarantola [11] or Tarantola [19]) and it is worth mentioning that they cannot admit every type of error probability distribution function (pdf hereafter). The normal pdf is for instance not appropriate.

In the next sections, we will encounter α and β prior guesses, β measurements and finally α and β optimal estimates. They all refer to the same physical entities (the correction functions) which are *Jeffrey's variables*. We decide hereafter to describe their error statistics with *the lognormal pdf* and this hypothesis is referred to as **H1**. This choice relies on the wide use of the lognormal pdf when handling positive variables but also essentially on the property attached to the above variable change:

$$\tilde{X} = \ln X \tag{5}$$

If the X error statistics is *lognormal* then the $\tilde{X}$ error statistic is *normal* [11, 19]. In the framework of the Maximum Likehood criterion and because of the assumption H1, such property justifies to develop the problem and optimize the J cost function with respect to $\tilde{X}$:

$$\tilde{X} = (\tilde{\alpha}, \tilde{\beta})^T = (\ln \alpha, \ln \beta)^T \tag{6}$$

$\tilde{X}$ is hereafter called the *control variable* or equivalently the correction function in the *control space*. The above described strategy will lead us to the well-known least-squares structure for the J cost function. At last, the ice age may now be expressed with respect to $\tilde{X}$:

$$\chi(z) = \int_0^z \frac{D(z') \exp \tilde{\alpha}(z') \exp \tilde{\beta}(z')}{S^b(z') T^b(z')} dz' \tag{7}$$

2.2 Discretized problem

The numerical treatment requires discretized depths which are designated by z_i with index i running from 1 to n, the size of the grid. To each ice layer lying between z_{i-1} and z_i are associated the above physical entities:

- its thickness $dz_i = z_i - z_{i-1}$,
- its relative density D_i (with respect to pure ice),
- the first guess values S_i^b and T_i^b,
- the related searched correction functions α_i and β_i,
- the related searched flow entities S_i and T_i,
- the corresponding control variable components $\tilde{\alpha}_i$ and $\tilde{\beta}_i$,

The discretization of the equation (7) leads to:

$$\chi_p(z_p) = \sum_{i=1}^{p} \frac{D_i \exp \tilde{\alpha}_i \exp \tilde{\beta}_i}{S_i^b T_i^b} dz_i \tag{8}$$

where χ_p is the ice age of the p^{th} discrete depth z_p and involves the corrected flow entities T and S by the mean of their respective correction functions $\exp \tilde{\alpha}$ and $\exp \tilde{\beta}$ (6).

[2] The reason being the size of X.

[3] Dated horizons,...

2.3 Cost function J

The J function makes a trade-off between the prior knowledge and the data constraint. We describe in the next sections the elements of this trade-off: 1) the prior information on X which is embodied first by a prior guess or *background vector* X^b and second by the *background error covariance matrix* B, 2) the observation model $h(X)$ which enables to predict the observations Y. The very classical assumption referred to as **H2** is made hereafter. It consists of no error correlation between the background and the observations. In this case, the cost function precisely splits in two terms [19]:

$$J(\tilde{x}) = J^{obs}(\tilde{x}) + J^b(\tilde{x}) \tag{9}$$

The first term J^{obs} measures the distance between the observations Y and the model predictions $h(X)$ while the second term J^b measures the distance between the searched and the prior correction functions X and X^b. Let us now detail the hypothesis and information necessary to derive the J^b and J^{obs} terms.

2.3.1 Background term J^b

The X^b vector is a part of the so-called *background* information which may be derived on the basis of the following rough statements. The background term aims during the optimization process at constraining T and S to remain "not too far from" T^b and S^b. In other words, J^b aims at maintaining the X vector "not too far from" 1 (see equations (3) and (4)) and this can be summarized with the above equation:

$$X^b = 1 \tag{10}$$

The true flow entities s^t and t^t and their associated true correction function x^t are unknowns. One obviously makes an error assuming that S^b, T^b and X^b are adequate estimates [4]. This error is the *background error* and we must now determine its nature.

The X^b vector being nothing else than a prior guess for X, on the basis of assumption H1 we apply the variable change of equation (5) to X^b and x^t. It introduces $\tilde{X}^b$ and $\tilde{x}^t$ from which one can reformulate the background choice (10) and define the *background error* in the *control space* $\tilde{\epsilon}^b$:

$$\tilde{X}^b = 0 \tag{11}$$
$$\tilde{\epsilon}^b = \tilde{X}^b - \tilde{x}^t \tag{12}$$

During the optimization process, the data constraint may drive away the $\tilde{X}$ value from the background vector choice (11) which therefore induces the so-called *background deviation*. The J^b term accounts for the cost of such *background deviation* by the mean of the B matrix which weighs each devitation component according to the confidence [5] attached to the background choice (11).

$$J^b(\tilde{x}) = \frac{1}{2}\left(\tilde{x} - \tilde{X}^b\right)^T B^{-1}\left(\tilde{x} - \tilde{X}^b\right) \tag{13}$$

The B matrix is defined with the $B = E[(\tilde{\epsilon}^b)(\tilde{\epsilon}^b)^T]$ statistics [6]. This statistical analysis may be performed for instance on more complex flow modelling [7]. This important work is however not in the scope of this study which purpose is essentially to describe and test this new dating method.

We therefore confine us to a very preliminary shaping on which will rely the numerical experiments shown in section 3. It requires to detail the block structure of the B matrix which relies on the two components $\tilde{\epsilon}^b_\alpha$ and $\tilde{\epsilon}^b_\beta$ [8] of the background error (12):

$$\begin{pmatrix} B_\alpha & B_{\alpha\beta} \\ B^T_{\alpha\beta} & B_\beta \end{pmatrix}$$

where B_α and B_β are the auto-covariance matrices related to $\tilde{\epsilon}^b_\alpha$ for the former and to $\tilde{\epsilon}^b_\beta$ for the latter, while $B_{\alpha\beta}$ is the cross-covariance matrix between $\tilde{\epsilon}^b_\alpha$ and $\tilde{\epsilon}^b_\beta$. On this basis, we assume first uncorrelated $\tilde{\epsilon}^b_\alpha$ and $\tilde{\epsilon}^b_\beta$ uncertainties which is hereafter referred to as assumption **H3**. The consequence is a null $B_{\alpha\beta}$ sub-matrix. This assumption is justified taking account of Parrenin et al. [14], who show that the total thinning function is only weakly sensitive to accumulation changes. This latter assumption greatly simplifies the $J^b(\tilde{x})$ expression which can split into two independent terms:

$$J^b(\tilde{x}) = J^b_\alpha(\tilde{\alpha}) + J^b_\beta\left(\tilde{\beta}\right) \tag{14}$$

where, when taking account of (11), $J^b_\alpha(\tilde{\alpha})$ and $J^b_\beta(\tilde{\beta})$ are given by:

$$J^b_\alpha(\tilde{\alpha}) = \frac{1}{2}\tilde{\alpha}^T B_\alpha^{-1}\tilde{\alpha} \tag{15}$$
$$J^b_\beta(\tilde{\beta}) = \frac{1}{2}\tilde{\beta}^T B_\beta^{-1}\tilde{\beta} \tag{16}$$

The shaping secondly consists to set independently the standard deviations (hereafter *std*) and the correlations:

$$[B_\alpha]_{ij} = \left[\sigma^b_\alpha\right]_i \left[\sigma^b_\alpha\right]_j \left[\rho^b_\alpha\right]_{ij} \tag{17}$$
$$[B_\beta]_{ij} = \left[\sigma^b_\beta\right]_i \left[\sigma^b_\beta\right]_j \left[\rho^b_\beta\right]_{ij} \tag{18}$$

[4] Flow models are imperfect.

[5] The B matrix is priorly involved in the gaussian pdf which measures the prior probability for $\tilde{X}$ to equate $\tilde{x}$ and from which with the Bayes theorem, is derived the J^b term.

[6] $E[.]$ is the expected value.

[7] One can mention the models that take account of: the anisotropy of the poly-crystalline ice, the horizontal shear for ice divide configurations, accumulation events not driven by water vapor amount dependence to temperature...

[8] $\tilde{\epsilon}^b_\alpha$ and $\tilde{\epsilon}^b_\beta$ are the background errors on each $\tilde{X}^b$ components which is to say $\tilde{\alpha}^b$ and $\tilde{\beta}^b$.

where σ_α^b and σ_β^b are the *std vectors* and ρ_α^b and ρ_β^b are the *correlation matrices* related to B_α and B_β . The precise std and correlation settings will be defined in section 3.

2.3.2 Observation term J^{obs}

Our experiments involve two types of observation designated as *age markers* and *correction markers*. We refer to them as the *assimilated observation* set. We call age markers any measurement enabling to associate an ice age to a given ice layer along the core. Correction markers are specific data enabling to infer corrections on the thinning function. They are estimated from the comparison of observed and modelled $\Delta depth$ which is the distance along the core separating concomitant gas and ice event [9]. The $\Delta depth$ can be estimated as the product of the thinning function $T(z)$ by the $codie(z)$ which is the initial thickness of the snow-firn column measured in meters of ice equivalent. In the bottom part of the core, we assume that the disagreements between the modelled and the observed $\Delta depth$ are due to errors on the thinning function rather than on the $codie$. This is a strong assumption hereafter referred to as **H5**.

In the next two paragraphs, we describe the observation components of the cost function. Because of the assumption (referred to as **H6**) of no error correlation between age markers and correction markers, J^{obs} reduces to a sum of two distinct terms J^a and J^c, related to age markers for the former and to correction markers for the latter:

$$J^{obs} = J^a + J^c \tag{19}$$

The H6 hypothesis is rather strong; in a more in-depth study, a careful examination of the origin of each data should be carried.

Age markers In order to detail the entities involved in the J^a term, we describe the age markers by a set of n_a triplets $(z_i^a, y_i^a, \sigma_i^a)$ with i running from 1 to n_a and where z_i^a is the depth for which the age y_i^a is observed with the σ_i^a std. The J^a term measures the distance between the observation vector y^a and $h^a(\tilde{x})$, the age marker *observation operator* [10]. Assuming normally distributed age marker errors, J^a can be written as follows:

$$J^a(\tilde{x}) = \frac{1}{2}\left(y^a - h^a(\tilde{x})\right)^T R_a^{-1}\left(y^a - h^a(\tilde{x})\right) \tag{20}$$

where R^a is the age observation *error covariance matrix* which is defined on one hand with the σ^a std vector and on the other hand with the ρ^a correlation matrix [11]:

$$[R_a]_{ij} = [\sigma^a]_i [\sigma^a]_j [\rho^a]_{ij} \tag{21}$$

The i^{th} component of $h^a(\tilde{x})$ is given by the following equation:

$$h_i^a(\tilde{x}) = \sum_{j=1}^{m_i^a - 1} \frac{\exp\tilde{\alpha}_j \exp\tilde{\beta}_j}{T_j^b S_j^b} D_j dz_j + \lambda_i^a \frac{\exp\tilde{\alpha}_{m_i^a} \exp\tilde{\beta}_{m_i^a}}{T_{m_i^a}^b S_{m_i^a}^b} D_{m_i^a} dz_{m_i^a} \tag{22}$$

The m_i^a index selects the $z_{m_i^a}$ depth which is the closest upper grid point to z_i^a (the depth axis being oriented toward the bedrock). Equation (23) involves a sum which runs from index 1 to index $m_i^a - 1$ and where the j^{th} term is the contribution of the j^{th} ice layer to the h_i^a value. The last term operates a linear interpolation between the depths $z_{m_i^a - 1}$ and $z_{m_i^a}$ through the λ_i^a factor:

$$\lambda_i^a = \frac{z_i^a - z_{m_i^a - 1}}{z_{m_i^a - 1} - z_{m_i^a}} \tag{23}$$

Correction markers The thinning correction markers are depicted by the set of n_c triplets $(z_i^c, y_i^c, \sigma_i^c)$ with i running from 1 to n_c and where y_i^c is the observed thinning correction for the z_i^c depth with an std estimate of σ_i^c. A correction marker being nothing else than the measurement for a specific depth of the thinning correction, it is also a Jeffrey's variable and on the basis of assumption H1 we apply the variable change of equation (5):

$$\tilde{y}_i^c = \ln(y_i^c) \tag{24}$$

where $\tilde{y}_i^c$ is the transformed i^{th} correction marker and has normally distributed errors. In this context, the correction markers induce a cost function term given by equation:

$$J^c(\tilde{x}) = \frac{1}{2}\left(\tilde{y}^c - h^c(\tilde{x})\right)^T R_c^{-1}\left(\tilde{y}^c - h^c(\tilde{x})\right) \tag{25}$$

where $h^c(\tilde{x})$ and R_c are the *observation operator* and *error covariance matrix* associated to the correction markers. The i^{th} component of h^c operator is:

$$h_i^c(\tilde{\beta}) = \sum_{j=1}^{n} \delta_{j,m_i^c} \tilde{\beta}_j \tag{26}$$

where, $\delta_{i,j}$ is the Kronecker symbol (which equals 1 when $i = j$ and zero otherwise) and the m_i^c index is such that $z_{m_i^c}$ is the closest upper grid point to z_i^c. Here again, R_c can be written in terms of the ρ^c correlation matrix and the σ^c std vector:

$$[R_c]_{ij} = [\sigma^c]_i [\sigma^c]_j [\rho^c]_{ij} \tag{27}$$

[9] At a given depth the gas trapped in the bubbles is younger than the surrounding ice.
[10] The h^a operator enables to predict y^a measurements.
[11] No error correlations being provided, the ρ^a matrix is therefore the identity.

2.3.3 Generalized observation operator and covariance matrix

In order to simplify the developments of section 2.4, we now define the *generalized observation operator* $h(\tilde{x})$:

$$h\left(\tilde{x}\right) = \begin{pmatrix} h^a\left(\tilde{x}\right) & 0 \\ 0 & h^c\left(\tilde{x}\right) \end{pmatrix} \tag{28}$$

According to H6, we also define R the *generalized observation error covariance matrix* which is diagonal-block:

$$R = \begin{pmatrix} R_a & 0 \\ 0 & R_c \end{pmatrix} \tag{29}$$

At last, $H\left(\tilde{x}\right) = \frac{\partial h}{\partial \tilde{x}}$ designates the *tangent linear operator* of the generalized observation operator.

2.4 Optimal solution and confidence intervals

The optimization of the cost function is performed with the m1qn3 minimizer developed by Gilbert and Lemarechal [3] which is based on a limited memory quasi-newton algorithm [2]. Let us designate $\hat{\tilde{x}}$ the optimized control variable. Assuming that the $h(\tilde{x})$ operator is only weakly non-linear (hypothesis **H7**), the confidence intervals on $\hat{\tilde{x}}$ can be estimated by the *posterior error covariance matrix* $\hat{\tilde{P}}$ [19] where $\hat{H}$ is the tangent linear operator estimated at the optimum $\hat{\tilde{x}}$:

$$\hat{\tilde{P}} \simeq \left(\hat{H}^T \tilde{R}^{-1} \hat{H} + \tilde{B}^{-1}\right)^{-1} \tag{30}$$

Let us write:

- $\hat{\chi} = \chi(\hat{\tilde{x}})$, the optimized ice chronology,
- $\nabla\hat{\chi}^T$, the related tangent linear operator calculated at the optimal point $\hat{\tilde{x}}$.

We now assume (hypothesis **H8**) that a normal pdf correctly approximates the uncertainties on $\hat{\chi}$ and we define:

$$Q = \nabla\hat{\chi}\tilde{P}\nabla\hat{\chi}^T \tag{31}$$

where the Q matrix is an approximation of the *posterior error covariance matrix* associated to the optimized ice chronology. The matrix diagonal elements consequently provide the confidence intervals on $\hat{\chi}$ (see appendix 5).

3 Applications: the EDC ice core

In this section we present numerical experiments on the EDC core, in order to test the new dating method. The first experiment consists in: 1) building an optimal age scale for the EDC core with the same elements used by Parrenin et al. [13] but in a more rigorous way 2) calculating the associated uncertainty. The two next experiments enable to investigate the sensitivity of the optimal age scale, the correction functions and the related confidence intervals to the shaping of the B matrix.

3.1 Standard experiment: EDC age scale construction

In order to construct an optimal age scale for the EDC core, we assimilate the whole set of age markers described in table 1 of Parrenin et al. [13], particularly the age markers of the core bottom which could not be respected with the Monte Carlo method (see introduction). We moreover use the optimized flow model simulations of Parrenin et al. [14] which provide us the prior guesses S^b and T^b. No correction markers are used for the current experiment.

The age marker std which are required to determine the R^a matrix are also taken from table 1 of Parrenin et al. [13]. No correlation between age observation errors were reported in [13] and we adopt this assumption. The R^a matrix is therefore diagonal. This can be a strong assumption in particular for age markers derived from an orbital tuning procedure like for instance the $\delta^{18}O$ data (O_2 isotope) which are used to derive the EDC3 age scale [13, 1]. The constant phase usually assumed in the tuning procedure may be wrong and therefore lead to a systematic bias.

As already detailed in section 2.3.1, a proper shaping of the B_α and B_β matrices would require a detailed statistical analysis. In this preliminary study we only propose some simplistic covariance modelling which are to a certain extend arbitrary and which we address in the next paragraph.

We first of all define the B_α covariances as functions of *age differences* while the B_β covariances are set as functions of *depth differences*. This separation is due to the distinct dependence of S^b and T^b either on age or on depth. Changes in the accumulation rate are not linked to the drilling depth but more naturally to the paleoclimate change through time whereas the thinning of an ice layer observed today along the core is more intrinsicly a mechanical state attached to the depth of the layer.

Let us secondly focus on the specific B_α settings. The error variance on $\tilde{\alpha}$ is assumed to be constant through time and for that purpose we set each σ_α^b vector components to 0.17. We do not expect the discrepancy between the "true" and the modelled accumulation to get worse in the past. We can however expect the model to better estimate the accumulation rates of the inter-glacial stages because the sedimentation model is derived from a present-day spatial parameterization linking the mean annual temperature with the ice deuterium content. We ignore this point in this preliminary study. In addition, the correlation matrix ρ_α^b is defined as a gaussian function of χ^b with L_α^b, a correlation length parameter in time unit which is set to 9 kyr (1 kyr = 1000 years):

$$\left[\rho_\alpha^b\right]_{ij} = \exp -\frac{1}{2}\left(\frac{\chi_i^b - \chi_j^b}{L_\alpha^b}\right)^2 \tag{32}$$

Let us at last detail the B_β settings. Referring to the $\tilde{\beta}$ error variance, its shape is chosen taking into account the two forward model characteristics: 1) the longer the ice particle trajectories, the greater the error of the forward

model is, 2) when dealing with a 1D flow model and depending on the amount of basal melting, the thinning function may become artificially very close to zero near the base; the potential result is a largely over-estimated ice age. In the light of this comment, one can control the magnitude of the error variance with the growth of the ice age and one candidate for the σ_β^b vector components can therefore be a growing function of the inverse of T_i^b, the total thinning experienced by the ice layer between z_{i-1} and z_i:

$$\left[\sigma_\beta^b\right]_i = \frac{\sigma_\beta^{b,0}}{H} \sum_{k=1}^{i} \frac{dz_k}{T_k^b} \tag{33}$$

where H is the total ice thickness and $\sigma_\beta^{b,0}$ a parameter which is set to 0.425. The related correlation profile is here again chosen as a gaussian function depicted with the corresponding correlation length parameter L_β^b set to 150 m:

$$\left[\rho_\beta^b\right]_{i,j} = \exp -\frac{1}{2}\left(\frac{z_i - z_j}{L_\beta^b}\right)^2 \tag{34}$$

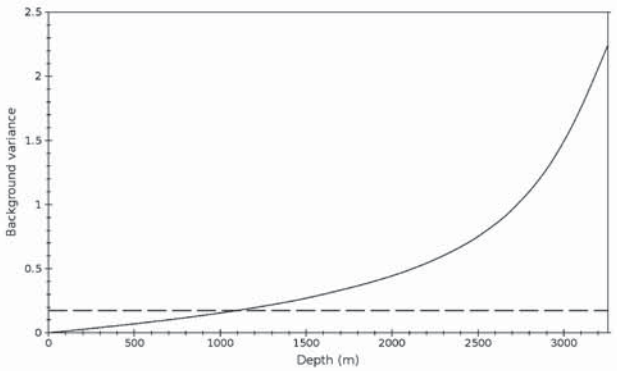

Figure 1: *Depth profiles for the background variances* $([\sigma_\alpha^b]_i)^2$ *(black dashed line) and* $([\sigma_\beta^b]_i)^2$ *(black solid line).*

These settings serve our numerical experiments. They induce a reversal of trend around 1000 m which is illustrated on Figure 1 with the σ_α^b and σ_β^b depth profiles. Below 1000 m because $\sigma_\beta^b > \sigma_\alpha^b$, the J function is more sensitive to a T deviation from its background T^b than to an S deviation from its background S^b while above 1000 m, the opposite configuration takes place. As a result, if corrections are necessary they will rather affect $\tilde{\alpha}$ below 1000 m and $\tilde{\beta}$ above.

The optimization of the cost function leads to the solution displayed on figure 2. On the top panel of the figure is plotted $\hat{\chi} - \chi^b$, the age difference between the optimized and the background age scale (black line) with the assimilated set of age markers and their uncertainty (black circles with error bars). The bottom panel operates a zoom in the depth interval lying between 2700 and 3255 m where the disagreement between the two ice chronologies is blazing. On this panel is directly compared the behavior of the two age scales with χ^b in grey dashed line and $\hat{\chi}$ in black solid line. Moreover, the uncertainty on the $\hat{\chi}$ optimized age scale is shown with a semi dashed red line on both panels.

3.2 Sensitivity experiment through covariance length changes

In order to investigate the sensitivity of the solution to the shaping of the error covariance matrices, we modify the B_β covariances by reducing the L_β value from 150 to 50 m (this affects the J^b terms and their weighing factors). We do not modify the other settings. The 1^{st} sensitivity experiment operates on the set of observations described above in the standard experiment whereas the 2^{nd} sensitivity experiment assimilates also thinning correction markers (see section 2.3.2). The aim of this latter experiment is to study how the β thinning correction and its confidence intervals behave in the neighborhood of β measurements. For that purpose, we use the $\Delta depth$ data discrepancies of table 2 in Dreyfus et al. [1] and we stick to the assumption H5 made in section 2.3.2. The observed $\Delta depth$ are deduced from warming or cooling events which are simultaneously recorded in the gas bubbles (greenhouse gases) and in the ice phase (through water isotope of ice which is a proxy of the temperature). Here again, we assume no correlation between correction marker errors. The R^c matrix is therefore diagonal. This may be a strong assumption if for instance the hypothesis of concomitant variations of the greenhouse and the temperature, reveals itself to be wrong.

In order to describe the results of the 1^{st} sensitivity experiment, we designate by $\hat{\chi}_{L_\beta=150}$ and $\hat{\chi}_{L_\beta=50}$ the two age scale solutions. Figure 3 compares their behavior. The set of age markers are still plotted as black circles with error bars. As for the standard experiment, we show on the top panel the two resulting age differences $\hat{\chi}_{L_\beta=150} - \chi^b$ (black dashed line) and $\hat{\chi}_{L_\beta=50} - \chi^b$ (grey solid line). The bottom panel operates a zoom below 2700 m and directly shows $\hat{\chi}_{L_\beta=150}$ and $\hat{\chi}_{L_\beta=50}$. On both panels are plotted the calculated uncertainties associated to each age scale, in red dashed line for $\hat{\chi}_{L_\beta=150}$ and in yellow solid line for $\hat{\chi}_{L_\beta=50}$.

Figure 4 displays the result of the 2^{nd} sensitivity experiment. The top and bottom panels show the $\hat{\beta}$ thinning correction function respectively for $L_\beta = 150$ and $L_\beta = 50$ m. The black squares with error bars are the thinning correction markers, the black line is the thinning correction function solution while the dashed black lines are the confidence intervals.

4 Discussion

On the two panels of figure 2, one can see how the optimized chronology does captures the necessary change of slope in order to respect the age markers. The general trend of the uncertainty on $\hat{\chi}$ is a growth (errors cumulate) on which are superimposed several drops localized in the neighborhood of age markers. These drops

markedly occur where the age marker uncertainty is below the uncertainty attached to the background age scale. This behavior can be observed for instance, between 2000 and 2700 m where 6 ages markers are assimilated with a 4 kyr uncertainty (see table 1 in Parrenin et al. [13]). This illustrates the expected spreading of the information brought by observations in their neighborhood. Further on, in area with high density of observations, the estimated age scale uncertainty is more or less steady but below the mean level of the related age marker uncertainties [12]: this feature can be clearly observed below 2700 m.

On the top panel of figure 3, the comparison of the $\hat{\chi}_{L_\beta=150}$ and $\hat{\chi}_{L_\beta=50}$ solutions shows a slight sensitivity of the age scales to L_β changes (in the investigated range). A smaller covariance length however leads to a chronology with smoother curvatures in the neighborhood of age markers. This feature can be observed on the two solutions $\hat{\chi}_{L_\beta=150}$ and $\hat{\chi}_{L_\beta=50}$, for the dated horizons lying at 1265.10, 1838.09 and 2620.23 m depth. It is meanwhile clear on both panels, that the uncertainty on the optimized age scale is strongly sensitive to L_β changes. One can expect that higher covariance lengths result in lower age scale uncertainty. This is however a little more complex because of two opposite driving forces. A greater covariance length: 1) causes the errors to cumulate faster with depth but 2) induces a wider diffusion of the information brought by an age marker. The latter statement is exclusively true when the age marker is in the scope of action of the covariance length. An illustration of this point can be observed below and above 2300 m. Below 2300 m, the uncertainty on $\hat{\chi}_{L_\beta=150}$ is first higher than the one related to $\hat{\chi}_{L_\beta=50}$ but then turns smaller downwards. Below 2300 m moreover, the depth interval separating two successive age markers is too large compared to the magnitude of the covariance length: the error accretion dominates and the uncertainty on the age solution is higher for $L_\beta = 150$ m [13]. Above 2300 m, this depth interval becomes sufficiently small compared to the magnitude of the covariance length: the spreading of data information dominates and the uncertainty on the age solution is lower for $L_\beta = 150$ m. This interpretation may be slightly blurred because in this experiment two covariance lengths operate at the same time: L_β and L_α. But above 2700 m the impact of the B_α covariances can be neglected regarding the respective magnitudes of: 1) σ_α and σ_β std, 2) L_α and L_β converted in age units [14]. Moreover the depth interval lying above 2700 m, characterized itself by uncertainties on age markers that are far below the uncertainty attached to the background age scale which ensures a strong inflexion of the uncertainty curve.

On figure 4, the expected behavior for the $\hat{\beta}$ solution and its confidence intervals [15] can be seen. At each correction marker depth, the uncertainty drops and the confidence intervals converge very close to the value of the uncertainty attached to the correction marker. The comparison of the two panels of figure 4 shows the impact of L_β changes: the larger the covariance length the further the uncertainty information brought by the correction marker data diffuses. One comment is necessary in order to explain the non smooth behavior of the solution at some particular depth, despite we do take into account correlations for the background errors. A detailed analysis shows that this behavior is observed when age marker constraint conflicts with a correction marker constraint, the former constraint requiring for instance an older ice age while the latter constraint pushes toward the opposite: this is precisely the case for the correction marker which is at 2785.75 m depth and the three age markers which are successively at 2789.58, 2799.36 and 2812.69 m depths (see tables 1 and 2 of Dreyfus et al. [13] and table 1 of Parrenin et al. [13]).

5 Conclusion

This paper detailed the technical frame of a new pragmatic inverse approach which optimally estimates the ice chronology of a given ice core. This inverse approach is new because it takes into account the ice flow model uncertainties. These latter cannot be ignored in the context of the simplified flow models currently used for inverse dating purpose, unless to enrich the flow models in order that they better describe the flow irregularities. The model uncertainty is introduced in a pragmatic way by the mean of correction functions targetting the total thinning function and the accumulation rate, two entities previously calculated with direct or already optimized dating simulations and which serve the purpose of prior guesses (or background) for the new inverse approach. A cost function is derived in a Bayesian framework which describes in a probabilistic way, the competition between the distance to the background knowledge and the distance to a set of observations. The optimization of the cost function enables to identify these correction functions and provides new estimates of the thinning function and the accumulation rate. Finally, these new flow entities lead to an optimal estimate of the ice age scale. In the Bayesian framework, the calculation of the solution confidence intervals can be performed under certain hypothesis.

We successfully applied this new dating method to construct the age scale of the EDC core with the use of the official set of age markers [13]. No a posteriori correction in the core bottom was needed: the new method enables in particular to respect the constraint of the $\delta^{18}O$ age markers which was not the case for the dating simulation optimized with a Monte Carlo technique. Besides,

[12] If some error correlations would have been taken into account between age markers, the observed uncertainty drop would not occur so markedly.

[13] More precisely, this comment holds above 500 m and below 2300 m.

[14] Around 2700 m, L_β becomes 2 (8) times larger than L_α for $L_\beta = 50$ (150) m while the σ_β std is 6 times larger than the σ_α std.

[15] The confidence intervals are absolute uncertainties. Their are however not symmetric with respect to the solution because they are calculated by the mean of the estimated relative uncertainty attached to the posterior lognormal error distribution.

the confidence interval associated to the new ice age scale behaves as expected: it increases with the distance to the nearest age marker.

Preliminary sensitivity tests confirm the well-known impact of the background error covariance matrices on the solution and especially on the estimated confidence interval: the larger the correlation lengths the further the information brought by a given observation propagates. One important task to do in future works is to shape with relevant physical information those background error matrices. A traditional but time consuming approach is to perform statistics on the outputs provided by some more complex flow modelling (full stokes or higher order models). Another approach would consist in working on small time intervals carefully chosen with a large number of observations and searching the most unfavorable shapes for the background error matrices which would however still respect the data set.

Some of the assimilated observations (i.e. data used to constrain the model) reveal our intent in a very close future, to inverse at the same time on the ice and on the gas age scale (correction markers are more rigorously $\Delta depth$ markers which are straightforwardly related to the close-off depth and $\delta^{18}O$ are gas rather than ice age markers). Here again, the idea is to use a prior guess for the $codie$ and to calculate an optimal correction function in best agreement with the data and the background knowledge. Moreover, the ability of the method to assimilate large set of observations brings the perspective to inverse chronologies of several cores simultaneously by using ice and gas stratigraphic links. This method will certainly provide a tool to the paleo-community, enabling to construct a common and optimal age scale for deep ice cores of Greenland and Antarctica.

Acknowledgements

This work was supported by the Agence Nationale de la Recherche (projects ANR-05-BLAN-0165-01). We are grateful to Michel Sacchettini for his technical help.

Appendix A : Confidence intervals on the optimal ice age

Let us call X, the model parameter vector to be identified in the framework of an inverse problem. Let us suppose we solve the problem with a variational approach with the minimization of J, the cost function of the problem. Let us call g, an additionnal observation model defined as an operator that maps the model space $\mathcal{M}$ into the observation space $\mathcal{D}$:

$$\begin{array}{rc} g: & \mathcal{M} \rightarrow \mathcal{D} \\ & x \mapsto y = g(x) \end{array} \tag{35}$$

Let us suppose that both $\mathcal{M}$ and $\mathcal{D}$ are linear spaces. If $X = x^t$ is the true but unknown optimal solution and if $X = \hat{x}$ is the estimated solution, one can define ϵ_x the analysis error as (assuming it to be normally distributed):

$$\epsilon_x = x^t - \hat{x} \tag{36}$$

with the associated P error covariance matrix:

$$P = <\epsilon_x {\epsilon_x}^T> \tag{37}$$

The true but unknown observation model can therefore be written as:

$$y^t = g\left(x^t\right) \tag{38}$$

while the estimated model is:

$$\hat{y} = g\left(\hat{x}\right) \tag{39}$$

The error made when estimating the true observation model to be $\hat{y} = g\left(\hat{x}\right)$ is given by ϵ_y:

$$\begin{array}{rcl} \epsilon_y & = & y^t - \hat{y} \\ & = & g\left(x^t\right) - g\left(\hat{x}\right) \end{array} \tag{40}$$

Let us suppose that $\epsilon_x = x^t - \hat{x}$ is small enough to write:

$$g\left(\hat{x} + \epsilon_x\right) - g\left(\hat{x}\right) = \hat{G}^T \epsilon_x + \circ\left(\|\epsilon_x\|\right) \tag{41}$$

where $\hat{G}^T$ is the tangent linear operator calculated at $X = \hat{x}$:

$$\hat{G}^T = [\frac{\partial g}{\partial X}]_{X=\hat{x}} \tag{42}$$

Equation (41) may be re-written using ϵ_y which is a randon function:

$$\epsilon_y = \hat{G}^T \epsilon_x + \circ\left(\|\epsilon_x\|\right) \tag{43}$$

Further on, assuming that ϵ_y is normally distributed, one can calculate Q, the error covariance matrix which measures the error made on y^t estimate:

$$\begin{array}{rcl} Q & = & <\epsilon_y {\epsilon_y}^T> \\ & = & <\hat{G}\epsilon_x {\epsilon_x}^T \hat{G}^T> \\ & = & \hat{G} <\epsilon_x {\epsilon_x}^T> \hat{G}^T \\ & = & \hat{G} P \hat{G}^T \end{array} \tag{44}$$

References

[1] G. B. Dreyfus, F. Parrenin, B. Lemieux-Dudon, G. Durand, V. Masson-Delmotte, J. Jouzel, J.-M. Barnola, L. Panno, R. Spahni, A. Tisserand, U. Siegenthaler, and M. Leuenberger. Anomalous flow below 2700 m in the EPICA Dome C ice core detected using $\delta^{18}O$ of atmospheric oxygen measurements. *Climate of the Past*, 3(2):341–353, 2007.

[2] J.C. Gilbert and C. Lemarechal. Some numerical experiments with variable-storage quasi-Newton algorithms. *Mathematical Programming*, 45(1):407–435, 1989.

[3] JC Gilbert and C. Lemarechal. The modules M1QN3 and N1QN3. *Program documentation, INRIA*, 1993.

[4] A. Grinsted and D. Dahl-Jensen. A Monte Carlo-tuned model of the flow in the NorthGRIP area. *Annals of Glaciology*, 35(1):527–530, 2002.

[5] P. Huybrechts, O. Rybak, F. Pattyn, U. Ruth, and D. Steinhage. Ice thinning, upstream advection, and non-climatic biases for the upper 89% of the EDML ice core from a nested model of the Antarctic ice sheet. *Climate of the Past*, 3(4):577–589, 2007.

[6] A.C. Lorenc. Analysis methods for numerical weather prediction. *Quarterly Journal of the Royal Meteorological Society*, 112(474):1177–1194, 1986.

[7] DG Martinson, NG Pisias, JD Hays, J. Imbrie, TC Moore, and NJ Shackleton. Age dating and the orbital theory of the ice ages: development of a high-resolution 0 to 300,000-year chronostratigraphy. *Quaternary Research*, 27(1):29, 1987.

[8] EPICA Community Members. Eight glacial cycles from an Antarctic ice core. *Nature*, 429:623–628, 2004.

[9] EPICA Community Members. One-to-one coupling of glacial climate variability in Greenland and Antarctica. *Nature*, 444:195–198, 2006.

[10] K. Mosegaard and A. Tarantola. Monte Carlo sampling of solutions to inverse problems. *J. Geophys. Res*, 100(B7):12–431, 1995.

[11] K. Mosegaard, A. Tarantola, et al. Probabilistic Approach to Inverse Problems. *International Handbook of Earthquake & Engineering Seismology, PartA*, pages 237–265.

[12] B. Narcisi, JR Petit, and M. Tiepolo. A volcanic marker (92 kyr) for dating deep East Antarctic cores. *Quat. Sci. Rev*, 25:2682–2687, 2006.

[13] F. Parrenin, J.-M. Barnola, J. Beer, T. Blunier, E. Castellano, J. Chappellaz, G. Dreyfus, H. Fischer, S. Fujita, J. Jouzel, K. Kawamura, B. Lemieux-Dudon, L. Loulergue, V. Masson-Delmotte, B. Narcisi, J.-R. Petit, G. Raisbeck, D. Raynaud, U. Ruth, J. Schwander, M. Severi, R. Spahni, J. P. Steffensen, A. Svensson, R. Udisti, C. Waelbroeck, and E. Wolff. The EDC3 chronology for the EPICA Dome C ice core. *Climate of the Past*, 3(3):485–497, 2007.

[14] F. Parrenin, G. Dreyfus, G. Durand, S. Fujita, O. Gagliardini, F. Gillet, J. Jouzel, K. Kawamura, N. Lhomme, V. Masson-Delmotte, C. Ritz, J. Schwander, H. Shoji, R. Uemura, O. Watanabe, and N. Yoshida. 1-D-ice flow modelling at EPICA Dome C and Dome Fuji, East Antarctica. *Climate of the Past*, 3(2):243–259, 2007.

[15] F. Parrenin, J. Jouzel, C. Waelbroeck, C. Ritz, and J.M. Barnola. Dating the Vostok ice core by an inverse method. *Journal of Geophysical Research. D. Atmospheres*, 106:31, 2001.

[16] F. Parrenin, F. Remy, C. Ritz, M.J. Siegert, and J. Jouzel. New modeling of the Vostok ice flow line and implication for the glaciological chronology of the Vostok ice core. *J. Geophys. Res*, 109, 2004.

[17] A.N. Salamatin, E.A. Tsyganova, V.Y. Lipenkov, and J.R. Petit. Vostok (Antarctica) ice-core timescale from datings of different origins. *Annals of Glaciology*, 39(1):283–292, 2004.

[18] A. Svensson, K. K. Andersen, M. Bigler, H. B. Clausen, D. Dahl-Jensen, S. M. Davies, S. J. Johnsen, R. Muscheler, F. Parrenin, S. O. Rasmussen, R. R??thlisberger, I. Seierstad, J. P. Steffensen, and B. M. Vinther. A 60 000 year Greenland stratigraphic ice core chronology. *Climate of the Past*, 4(1):47–57, 2008.

[19] A. Tarantola. Inverse Problem Theory and Methods for Model Parameter Estimation (Philadelphia, PA: SIAM). 2005.

[20] F. Traufetter, H. Oerter, H. Fischer, R. Weller, and H. Miller. Spatio-temporal variability in volcanic sulphate deposition over the past 2 kyr in snow pits and firn cores from Amundsenisen, Antarctica. *Journal of Glaciology*, 50(168):137–146, 2004.

[21] YJ Wang, H. Cheng, RL Edwards, ZS An, JY Wu, C.C. Shen, and JA Dorale. A High-Resolution Absolute-Dated Late Pleistocene Monsoon Record from Hulu Cave, China. *Science*, 294(5550):2345, 2001.

Figure 2: *Standard experiment: ice chronology of the EDC core and its confidence interval calculated with the new dating method. The top panel covers the whole chronology while the bottom panel operates a zoom between 2700 m and the core bottom. The ages are measured in kyr (1000 years). The age difference between the new and the background chronology is shown in solid black line on the top panel while the bottom panel directly shows the new and the background age scales using the same color code (related Y-axis on the left); on both panels, in red dashed line is plotted the related estimated age scale uncertainty (related Y-axis on the right) as well as the assimilated age markers in black circles with error bars.*

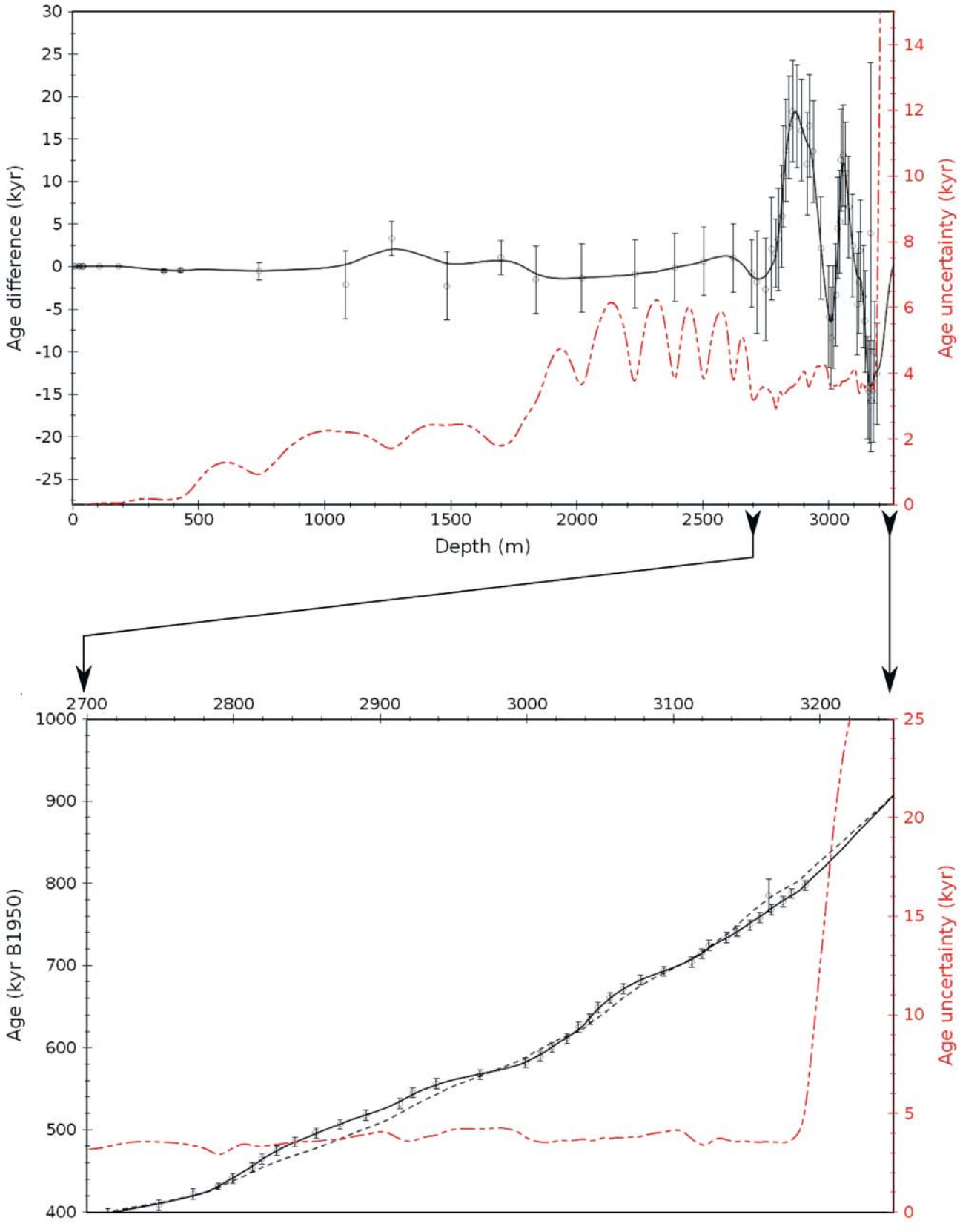

Figure 3: 1^{st} *sensitivity experiment: EDC ice chronologies and their related uncertainties calculated with two covariance lengths* $L_\beta = 150$ *and* $L_\beta = 50$ *m. The top panel covers the whole chronology while the bottom panel operates a zoom between 2700 m and the core bottom. The ages are measured in kyr (1000 years). The age differences between the new and the background chronologies are shown on the top panel, for both covariance length* $L_\beta = 150$ *m (black dashed line) and* $L_\beta = 50$ *m (grey solid line) while the bottom panel directly shows both age scales using the same color code (related Y-axis on the left); on both panels, in red dashed line and yellow solid line are plotted the estimated age scale uncertainties respectively for* $L_\beta = 150$ *and* $L_\beta = 50$ *m (related Y-axis on the right) while black circles with error bars are the assimilated age markers.*

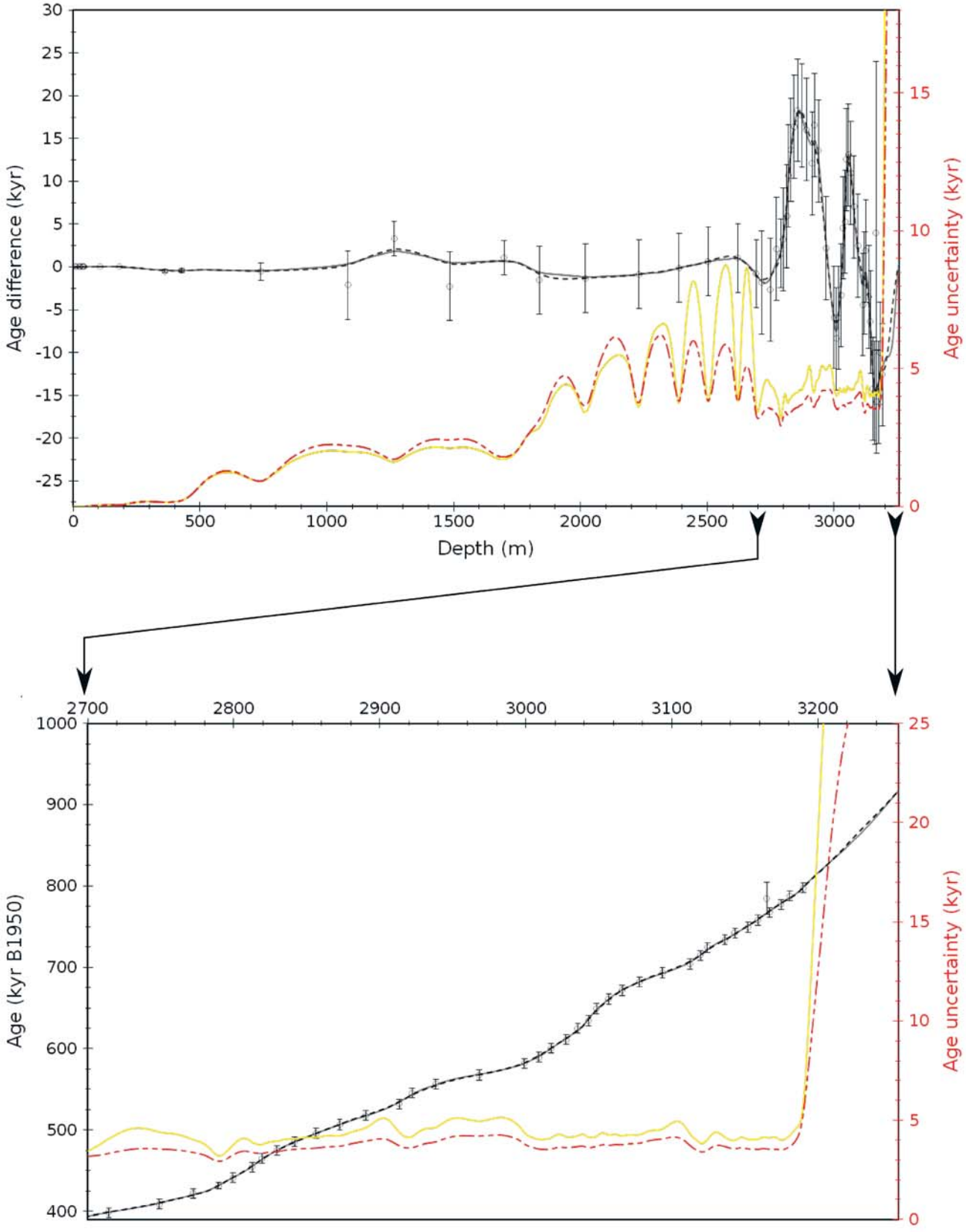

Figure 4: 2^{nd} *sensitivity experiment: thinning function correction calculated for two covariance lengths* $L_\beta = 150$ *and* $L_\beta = 50$ *m. On the top panel,* $L_\beta = 150$ *m while on the bottom panel* $L_\beta = 50$ *m. The squared markers with error bars are the thinning correction observations (the correction markers) and their uncertainty. The black solid line is the estimated thinning correction function while the black dotted lines are the related confidence intervals.*